

Nanoscale

Accepted Manuscript

This article can be cited before page numbers have been issued, to do this please use: A. Serfz, G. A. Csík, A. Kormanyos, A. Balog, C. Janaky and B. Endrői, *Nanoscale*, 2023, DOI: 10.1039/D3NR03834C.



This is an Accepted Manuscript, which has been through the Royal Society of Chemistry peer review process and has been accepted for publication.

Accepted Manuscripts are published online shortly after acceptance, before technical editing, formatting and proof reading. Using this free service, authors can make their results available to the community, in citable form, before we publish the edited article. We will replace this Accepted Manuscript with the edited and formatted Advance Article as soon as it is available.

You can find more information about Accepted Manuscripts in the [Information for Authors](#).

Please note that technical editing may introduce minor changes to the text and/or graphics, which may alter content. The journal's standard [Terms & Conditions](#) and the [Ethical guidelines](#) still apply. In no event shall the Royal Society of Chemistry be held responsible for any errors or omissions in this Accepted Manuscript or any consequences arising from the use of any information it contains.

One-step electrodeposition of binder-containing Cu nanocube catalyst layers for carbon dioxide reduction

Andrea Serfőző,^a Gábor András Csík,^a Attila Kormányos,^a Ádám Balog,^a Csaba Janáky,^a Balázs Endródi^{*a}

Received 00th January 20xx,
Accepted 00th January 20xx

DOI: 10.1039/x0xx00000x

To reach industrially relevant current densities in the electrochemical reduction of carbon dioxide, this process must be performed in continuous-flow electrolyzer cells, applying gas diffusion electrodes. Beyond the chemical composition of the catalyst, its morphology, and the overall structure of the catalyst layer are both decisive in terms of reaction rate and product selectivity. We present an electrodeposition method for preparing coherent copper nanocube catalyst layers on hydrophobic carbon papers, hence forming gas diffusion electrodes with high coverage in a single step. This was enabled by the proper wetting of the carbon paper (controlled by the composition of the electrodeposition solution) and the use of a custom-designed 3D-printed electrolyzer cell, which allowed to deposit copper nanocubes selectively on the microporous side of the carbon paper substrate. Furthermore, a polymeric binder (Capstone ST-110) was successfully incorporated in the catalyst layer during electrodeposition. The high electrode coverage and the binder content together result in an increased ethylene production rate during CO₂ reduction, as compared to catalyst layers prepared from simple aqueous solutions.

Introduction

Electrochemical reduction of carbon dioxide (CO₂RR) has been undoubtedly among the most intensively studied electrochemical processes in recent years.^{1,2} The large number of researchers working in the field brought a notable progress in understanding the reaction mechanisms, identifying active and selective catalysts, and developing efficient electrolyzer cells, stacks. This latter becomes more and more important, as the industrial implementation of CO₂RR seems to be feasible in the close future.^{3–6}

The maximum rate of CO₂RR in aqueous solutions is limited by the solubility of CO₂, which is around 30 mM at room temperature. The mass transport of CO₂ in such solutions limits the maximum current density to a few tens of mA cm⁻² for 2 electron products (i.e., carbon monoxide, formate).⁷ Furthermore, a large cell voltage develops due to the large distance between the electrodes in the cells typically used in laboratory experiments (e.g., H-cells). Finally, the product separation from the solution (in case of formate) in batch reactors is challenging. These obstacles can be overcome by using continuous-flow electrolyzer cells.⁸ Here, CO₂ is fed to the cathode catalyst through a porous substrate, the gas diffusion layer (GDL), hence decreasing the diffusion layer thickness by several order of magnitudes.⁹ The distance between the electrodes is minimized, and they are typically separated by only a membrane (zero-gap electrolyzer cells), a thin liquid electrolyte (microfluidic electrolyzer cells), or two liquid electrolytes and a membrane (hybrid electrolyzer cells).¹⁰ GDLs are typically formed of two layers: a macroporous layer, with larger pore size for gas transport, and a microporous layer. The GDL with catalyst-coated microporous layer is called the gas diffusion electrode (GDE), which is the central piece of

electrolyzer cells.¹¹ The structure of this GDE assures the proper reactant and product transport. It is mechanically stable and electrically conductive, assuring low cell resistance. A further important role of the GDE is to separate the gas and liquid phases, hence avoiding gas breakthrough or electrode flooding.^{12,13} For this reason, the typically applied GDLs are impregnated with hydrophobic compounds, such as polytetrafluoroethylene (PTFE). GDEs are usually formed by physical means, immobilizing nanoparticles on GDLs by spray-coating, drop-casting, sputtering, or other alternative techniques.^{11,14} Electrodeposition is another possibility for GDE preparation. In this case, the catalyst layer is directly formed on the microporous side of the GDL, hence a low contact resistance – and the formation of a strongly adhering layer is expected. Furthermore, electrochemical methods allow to precisely tune the amount of the deposited catalyst, simply controlling the deposition time, charge, or cycle number (in case of dynamic electrodeposition methods). Also, the electrodeposition conditions dictate the morphology, crystallinity, and size of the forming catalyst particles and layer.^{15–18} Finally, electrodeposition is relatively easy to be scaled-up to form large-area electrodes.¹⁹

Copper is one of the most frequently studied catalysts for CO₂RR, rooted in its unique capability to form C₂+ products from CO₂ in a single step. The selectivity is highly dependent on the catalyst morphology and the exposed crystal facets.^{20–22} Among other morphologies, copper nanocubes (Cu NCs) offer high selectivity for ethylene production in CO₂RR.^{23–28} The selectivity is affected by the size of the catalyst particles that can be tuned by varying the synthesis parameters. Electrodeposition is a versatile method in this regard, as the reaction conditions (e.g., precursor concentration, overpotential) were proven to control the forming catalyst layer, and consequently the reaction rate and selectivity.^{29–31} We note that the main drawback of using Cu NCs for CO₂RR is the morphological change of the catalyst during the reaction. Different mitigation strategies are being pursued at multiple research groups to avoid this, including the deposition of organic or inorganic protective coatings on the nanoparticles.³²

^a Department of Physical Chemistry and Materials Science, University of Szeged, Rerich Square 1, Szeged, H-6720 Hungary

*E-mail: endrodib@chem.u-szeged.hu (B. Endródi)

†Electronic Supplementary Information (ESI) available: [Further characterization of the catalyst layers]. See DOI: 10.1039/x0xx00000x



Stabilization of these particles is, however, beyond the scope of this contribution. Here we focus on the electrochemical formation of GDEs, and apply Cu NCs as a model system.

Performing electrodeposition from aqueous electrolyte solutions is not straightforward on the typically used GDLs, due to their hydrophobicity. It is not even trivial to immerse such substrates in water-based solutions. Applying apolar organic solvents, which fully wet the GDL, on the other hand, leads to the penetration of the electrolyte solution in the deeper pores, where electrodeposition might also occur. In this case, the pore structure of the GDL can be distorted, which should be avoided. Here we demonstrate on the example of Cu NC catalysts how the microporous side of a hydrophobic GDL can be selectively and fully coated via electrodeposition, by tailoring the precursor solution composition and using a simple 3D-printed electrodeposition cell. Furthermore, we show that a binder material (Capstone ST-110 polymer in this case) can also be incorporated in the catalyst layer in the same single electrodeposition step. The electrocatalytic activity of the formed layers are compared based on CO₂RR experiments in a continuous-flow microfluidic electrolyzer cell. Overall, the approach presented here to form fully covered, binder containing GDEs is expected to be generally applicable for different GDL-catalyst systems.

Experimental section

Materials

All chemicals used in this study were purchased from Sigma-Aldrich or VWR International. Chemicals of high purity (at least ACS reagent grade) were purchased and used without further purification. Ultrapure water (18.2 MΩ cm) was used for the experiments, freshly produced using a Millipore Direct Q3 UV instrument. A 4.5 purity CO₂ gas was employed in the CO₂RR studies.

Catalyst electrodeposition on gas diffusion layers (GDLs)

Electrodeposition of the catalyst layers was performed in a custom designed, 3D-printed electrolyzer cell (see **Fig. 1**). A Raise3D N2 type 3D printer was used to manufacture the cell components. Cells were printed from an acrylonitrile butadiene styrene polymer (ABS), with 100% filling ratio to ensure the liquid and gas tightness of the cell. A regular three electrode arrangement was applied for the electrodeposition, in which a Ag/AgCl/3M NaCl electrode and a copper mesh served as reference and counter electrodes, respectively, while a Freudenberg H23C6 type GDL was used as working electrode. Importantly, only the microporous side of the GDL is in direct contact with the electrolyte solution, hence enabling to selectively deposit the catalyst layer on that side. The anode electrodes were made by spray-coating a suspension of commercial Ir powder (1:1 isopropanol/water mixture as solvent, 15 wt% Nafion ionomer content as referred to the total Ir+binder amount, Ir concentration of 20 mg cm⁻³) on a Freudenberg H23C6 GDL, with a catalyst loading of 1 mg cm⁻².

The electrodeposition experiments have been carried out using a Metrohm Autolab 204 type instrument. DOI: 10.1039/D3NR03834C

Physical characterization of the samples

A Thermo Scientific Apreo 2 scanning electron microscope (SEM) was employed to collect information on the morphology of the formed electrodes. A Krüss EasyDrop instrument was used to measure the wetting properties (that is, contact angles) of different solvent mixtures on the microporous side of the Freudenberg H23C6 GDL. A droplet of the solvent mixture was formed on the plate using a syringe. Using the CCD camera of the goniometer, the drop contour of the captured photographs was analysed. The pH of the solutions was measured using a Mettler Toledo FiveEasy Plus FP20 pH meter.

Measurements in a continuous-flow electrolyzer cell

Continuous-flow electrolysis experiments were performed in a two-electrode setup employing a microfluidic cell designed based on the work of the Kenis research group.^{33,34} This consisted of two stainless steel electrode contacts, separated by a single poly(methyl methacrylate) (PMMA) flow channel (d = 2 mm thickness). 3 mm deep cavities were formed on the metal electrodes to serve as gas flow channels. An inlet and an outlet port were added to the cathode current collector for CO₂ transport, while a single outlet port was formed on the anode for the evolving O₂. A 2 cm x 0.5 cm large opening was created in the middle of the PMMA separator, defining A = 1 cm² electrolysis geometric area. Ø = 1 mm holes were drilled in two opposite sides of this plastic element, going through the middle of the formed opening, for the transport of the electrolyte solution. The connection for the liquid pump was established by mounting 1 mm needles in the holes. The cathode GDE, together with a PTFE gasket around it, was mounted between the cathode electrode and the plastic flow element. The anode was mounted in the cell similarly. CO₂ gas was fed to the cathode in a flow-by mode at a rate of u = 20 sccm, while a 1 M KOH electrolyte was directed between the two electrodes at a flow rate of 0.5 cm³ min⁻¹. A Bronkhorst EL-FLOW Select F-201CV mass flow controller and a KF Technology NE-300 syringe pump was used for was used for regulating the gas and the liquid flow rate, respectively. The electrochemical measurements were controlled using a Biologic VMP300 type instrument. The CO₂RR products were monitored during the electrolysis using a Shimadzu GC-2030 Plus gas-chromatograph (operated with 6.0 He carrier gas), equipped with a barrier discharge ionization (BID) detector and an automatic 6-way valve injection system. Faradaic efficiency of the CO₂ electrolysis was calculated from the GC results and the measured gas flow rate (Agilent ADM flow meter). Importantly, the pressure increase in the gas line – that could lead to electrode flooding – was avoided by applying a small vacuum pump to fill the sample loop of the injector, sampling the main gas stream.



Results and discussion

An electrodeposition cell was designed to ensure that electrodeposition of the catalyst layer occurs only on the microporous side of the GDL (Fig. 1). This is achieved by mounting the GDL between the plastic backplate of the cell and a gasket, on which an opening defines the electrode area that is in contact with the liquid electrolyte. Importantly, if the solution is not wetting the GDL fully, any electrochemical (Faradaic) process can only occur on the surface. This cell design is based on the cells typically applied in anodization studies,^{35,36} and it was prepared by 3D printing. Importantly, this allowed us to scale the electrolyzer cell to the desired electrode size rapidly.

Electrodeposition of Cu nanocube (Cu NC) layers was based on previous pioneering studies.^{29–31} As a first step, we used aqueous CuSO₄/KCl solutions, and successfully implemented their deposition protocol, leading to the formation of Cu NCs catalysts. We found, however, that the coverage of the GDL was low, approximately 15–20% of the total surface area. This is related to the hydrophobicity of the GDL's microporous layer, which is not wetted by the solution.

To overcome this challenge, based on our earlier experience,³⁷ we applied isopropanol : water (IPA : H₂O) solvent mixtures instead of pure water. Increasing the IPA content of the solution led to improved surface wetting (i.e., decreasing contact angle) of the microporous surface of the GDL (Fig. 2). We note that there is a fine balance here: while proper wetting of the surface is a prerequisite for fully coated GDE preparation, the electrolyte solution should not penetrate the deeper pores of the GDL, as this would lead to catalyst deposition throughout the GDL. This latter could distort the gas transport and affects the flooding properties of the GDE during CO₂RR, the targeted application for these electrodes. The amount of the depositing material was regulated by the number of cycles. The deposition was performed from a solution containing CuSO₄ and KCl at the same concentration.

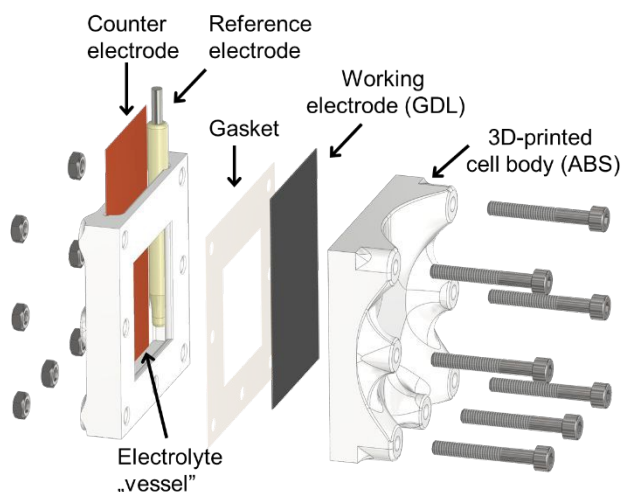


Fig. 1. Schematic drawing of the 3D-printed electrolyzer cell used for the electrodeposition of the Cu NC catalyst layers on the microporous side of hydrophobic GDLs. The opening where the GDL surface is in contact with the electrolyte solution is 3.5 cm × 3.5 cm large.

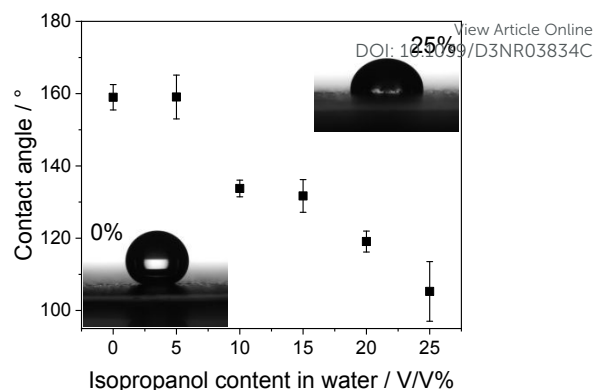


Fig. 2. Contact angles of different water/isopropanol solvent mixtures on the microporous side of a Freudenberg H23C6 GDL.

Electrodeposition was performed via a potentiodynamic method, applying the same potential limits as in ref.³⁰ (between +0.55 V and +0.22 V, both vs. RHE) (Fig. 3A). Low deposition currents were observed at very low concentrations (1 mM), related to the mass transfer limitations arising in the quiescent solution. The deposition rate increases with the increasing precursor concentration, caused by the increased mass transport rate and decreased solution resistance. As an illustrative example, we compare here the morphology of the layers formed from 5 mM CuSO₄/KCl solution in pure water and in 15 V/V% IPA containing aqueous solutions, applying the same number of deposition cycles (Fig. 3B and C, respectively). In agreement with former reports,^{29–31} we confirmed the deposition of Cu NCs using pure water as solvent (Fig. 3B). The formation of densely covered and “empty” regions were observed on the SEM images, and the surface coverage was estimated to be around 15–20%. In stark contrast, an almost fully covered surface was witnessed when the solvent mixture contained 15 V/V% IPA (Fig. 3C and Fig. S1). Importantly, the cube morphology was observed in this case as well. This proves our hypothesis, namely that *by tailoring the solvent composition, the surface coverage of the electrode can be tuned during electrodeposition*. As for the effect of the varying solvent composition, we performed studies with different IPA : H₂O mixtures, at a constant precursor concentration. In agreement with the contact angle measurements (Fig. 2), an increasing surface coverage was observed up to 15% IPA content. At higher IPA contents, however, a gradually decreasing amount of catalyst deposition was observed on the GDL surface, and the cube morphology was also distorted, the formation of platelets was seen (Fig. S2). This is caused by the penetration of the solution in the pores of the GDL, hence the deposition occurs there as well. A high capacitive current appeared in this case, due to the large inner surface area of the porous substrate (Fig. S3).³⁸ Under the applied potentiodynamic conditions, only small fraction of the total charge is consumed in a Faradaic process (i.e., the deposition of copper nanoparticles). Furthermore, a gradual decrease of the particle size was also witnessed with the increasing IPA ratio (Fig. S4). This causes an increase in the surface area of the catalyst particles, hence a larger number of exposed crystal edges that can result in higher CO₂RR activity and selectivity.



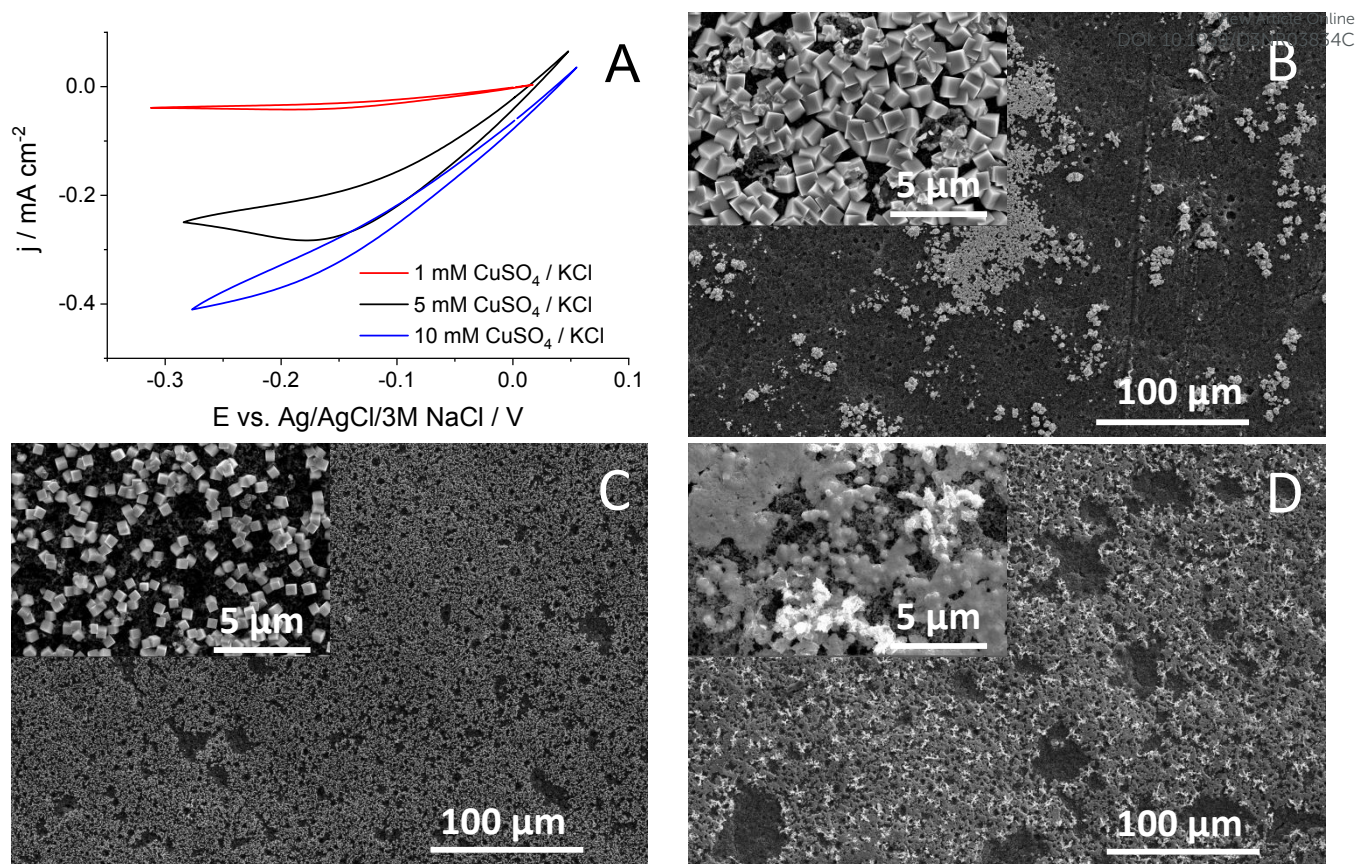


Fig. 3. (A) Representative potentiodynamic curves recorded for Cu NC synthesis on Freudenberg H23C6 GDL. The sweep rate was $v = 100 \text{ mV s}^{-1}$, and the measurements were performed at room temperature, in 15 V/V% isopropanol containing aqueous solutions. SEM images taken at two different magnifications (see the insets) of layers deposited from 5 mM CuSO₄/KCl solutions; in (B) pure water (C) 15 V/V% isopropanol containing solvent mixture (D) from a solution identical to (C), but also containing 100 mg/l Capstone ST-110. 500 electrodeposition cycles were applied for (B), (C) and (D). The integrated charge during the depositions varied within a 20% range.

Furthermore, this also implies the decrease of the layer thickness, as under the applied conditions, a “monolayer” of Cu nanocubes form on the GDLs. We also mention that the formation of larger copper aggregates is typically seen on the layers formed from pure water, while these structures are absent when a solvent mixture that wets the GDL fully, is used (Fig. S5). All further measurements were performed applying pure water or 15% IPA containing solutions, and 5 or 10 mM CuSO₄ concentration. The Cu NC catalyst containing GDEs were tested in CO₂RR in a microfluidic electrolyzer cell,^{39,40} in galvanostatic measurements (Fig. 4, Table S1). Comparing the cell voltage stability using the GDEs formed from pure water and in the 15% IPA:water mixture a striking difference is seen, even without analyzing the formed products. While stable cell voltages were recorded in the latter case, the GDE formed from pure water failed rapidly at the highest studied current density (200 mA cm⁻²), signalled by the large decrease (from ca. 3.2 V to ca. 2.6 V) of the cell voltage (Fig. 4A). This is caused by the flooding of the GDE, and the consequent dominance of cathodic HER, which proceeds at a less negative potential compared to CO₂RR. We believe that the rapid cell failure is rooted in the high local current densities at the catalyst covered parts of the GDE; note that the current density is normalized by the geometric surface area of the GDE. However, as only 15-20% of the surface is coated with Cu NCs, the 200 mA cm⁻² geometric area normalized current density translates to 1-1.3 A cm⁻² catalyst geometric area normalized current density. This high current density can cause rapid catalyst degradation, increased

local temperature and electrowetting, which together lead to the flooding of the GDE.

Irrespective of the solvent used during the electrodeposition of Cu NCs, ethylene was the dominant CO₂RR product in the gas phase, while methane and carbon monoxide were detected in small concentration on all GDEs (Fig. 4B). As expected from the low surface coverage, relatively low CO₂RR reduction rate was measured for the GDEs formed applying pure water as solvent. At 200 mA cm⁻² current density HER was the dominant electrode process, proceeding with ca. 75% Faradaic Efficiency (FE), independent from the CuSO₄/KCl concentration.

HER was efficiently suppressed on the GDEs deposited from IPA:water mixtures. The FE(H₂) was between 10-15% at all studied current densities. In parallel to this, FE(C₂H₄) was between 45-50%, with slightly lower values measured for the samples prepared at lower precursor concentrations. At higher current densities a notable ethanol (FE ~5-6%) and acetate (FE ~3-4%) formation rates were witnessed for these GDEs.

To increase the stability of the electrodeposited layers, we aimed to incorporate a binder in the catalyst layer during electrodeposition. Therefore, the electrodeposition of the catalyst layers was repeated from 15 V/V% IPA containing precursor solutions, containing also different amounts of Capstone ST-110, a commercial pore sealer.⁴⁰ This resulted in the formation of a coherent layer between the Cu NCs, implying the incorporation of the polymer (Fig. 3D and Fig. S6-7).



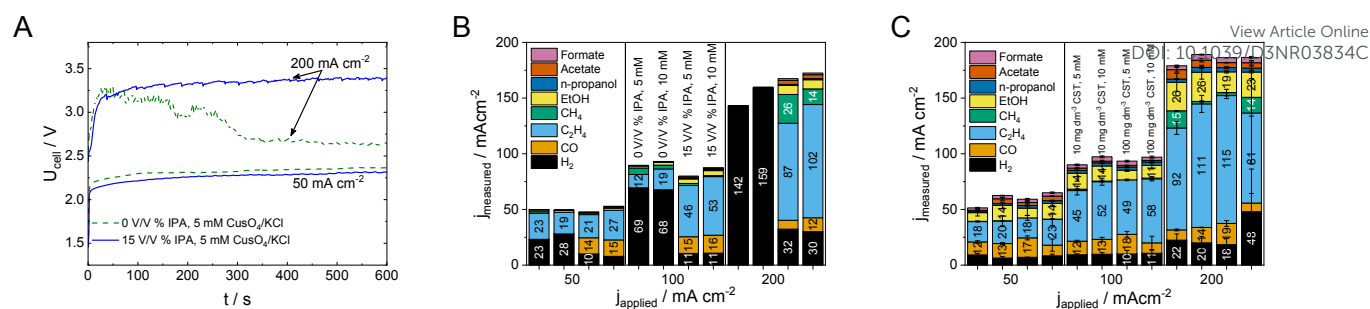


Fig. 4. (A) Typical galvanostatic CO₂RR measurements with Cu NC catalyst layers formed from solutions of identical precursor concentration, using pure water or 15 V/V% IPA in water mixture as solvent. Product distribution during galvanostatic CO₂RR experiments on Cu NC catalyst layers electrodeposited (B) from pure water or 15 V/V% IPA containing solution, (C) from solutions in 15 V/V% IPA in water mixture, also containing different amount of Capstone ST110 ionomer. The experiments in (B) and (C) were performed at both 5 and 10 mM CuSO_4/KCl concentrations. All measurements were performed at room temperature in a microfluidic electrolyzer cell, with a cathodic CO_2 feed of $20 \text{ cm}^3 \text{ min}^{-1}$ and with a 1 M KOH solution flowing between the electrodes at a rate of $0.5 \text{ cm}^3 \text{ min}^{-1}$. All GDEs were formed by 500 times repeating the potentiodynamic deposition protocol shown in Fig. 3A.

This polymer layer thickness increases with the binder concentration in the precursor solution but has no clear effect on the crystal size of the forming particles, suggested by the almost identical XRD patterns (Fig. S7). When testing these layers in CO₂RR (Fig. 4C), a further increased ethylene ($\text{FE}(\text{C}_2\text{H}_4)$ above 55%) and ethanol ($\text{FE}(\text{EtOH})$ between 10-15%) formation selectivity was witnessed, and the HER was further suppressed ($\text{FE}(\text{H}_2) \leq 10\%$). Interestingly, a lower polymer content was found to be beneficial for the layers deposited from higher concentration precursor solutions, while a higher CST concentration resulted in better selectivity for the layers formed at lower CuSO_4 concentration. We attribute this trend to the differences in the particle size of the Cu NCs (Fig. S8). Importantly, the measured selectivity greatly exceeds that gathered with commercial Cu nanopowder ($\text{FE}(\text{C}_2\text{H}_4) \approx 35\%$) under identical conditions (Fig. S9).

The stability of the catalyst layers formed from pure water solvent, and from IPA and CST containing solutions was compared in constant current electrolysis experiments at $j = 200 \text{ mA cm}^{-2}$ (Fig. 5A,B, Table S1). In these studies, an almost instantaneous flooding of the former was experienced, while a constant ethylene formation rate with $\text{FE}(\text{C}_2\text{H}_4)$ between 57-60% was observed on the polymer containing GDE for ca. 45 minutes, when flooding of the layer occurred, as shown by the rapid cell voltage decrease.

We note that these experiments were repeated a few times, resulting in very similar conclusions, although with slightly varying time until flooding. We attribute the eventual flooding to the degradation of the Cu NCs. According to our SEM studies, the initial structure in which both the cube morphology and a polymer coverage can be observed changes during the reaction, resulting in the damage of the coherent catalyst layer, exposing larger area of the GDL (Fig. 5C). Although we expect that further tuning the layer thickness and the deposition solution composition the lifetime of such catalyst layers could be extended. However, the degradation of

Cu NCs will eventually occur,⁴¹ and therefore we did not attempt to extend this study in this direction.

Conclusions

Tailoring the solvent mixture composition, ideal wetting of the surface of a hydrophobic GDL can be achieved. Performing electrodeposition from such solution mixture leads to high and homogeneous surface coverage, as demonstrated on the example of copper nanocubes (Cu NC). Importantly, when performing the same electrodeposition from pure water, only 15-20% of the substrate was coated with catalyst, while using fully wetting solvent the electrodeposition occurred within the GDL, blocking the pores that are pivotal for proper gas transfer, and distorting the structure of the substrate. Increasing the surface coverage resulted in better performance in CO₂RR performed in a continuous-flow microfluidic electrolyzer cell, that was demonstrated by the better tolerance against flooding, and the higher formation rate of C₂+ products (ethylene in particular). Performing the electrodeposition with a polymeric binder added to the precursor solution, Capstone ST-110 binder-containing catalyst layers could be deposited. A slightly increased C₂+ selectivity was witnessed using these catalyst layers for CO₂RR. More importantly, the stability of the layers increased due to the homogeneous GDL coverage and the binder incorporation. Although a specific example is shown here to highlight the benefits of electrochemically forming GDEs from solutions of tailored composition, we believe that this strategy can be extended to other systems as well. Electrodeposition is highly controllable and fairly easily scalable method, hence it can offer an alternative to prepare large area GDEs for CO₂ electrolyzers, while also avoiding any physical catalyst immobilization steps (e.g., spray-coating). This offers faster GDE preparation, and fully circumvents any possible contamination originating from the physical deposition of the catalyst.



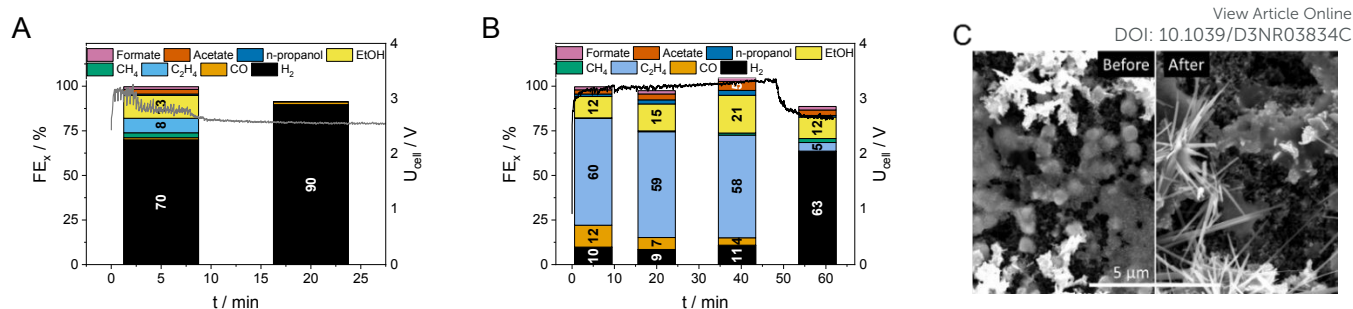


Fig. 5. Constant current electrolysis experiments at $j = 200 \text{ mA cm}^{-2}$ using GDEs formed from a 5 mM CuSO_4/KCl containing solutions in (A) pure water, (B) 100 mg/l CST and 15 V/V% IPA containing aqueous solution with 500 deposition cycles. All measurements were performed at room temperature in a microfluidic electrolyzer cell, with a cathodic CO_2 feed of $20 \text{ cm}^3 \text{ min}^{-1}$ and with a 1 M KOH solution flowing between the electrodes at a rate of $0.5 \text{ cm}^3 \text{ min}^{-1}$. All GDEs were formed by 500 times repeating the potentiodynamic deposition protocol shown in Fig. 3A. (C) SEM images taken of the GDE deposited from IPA and CST containing solutions, before and after the electrochemical measurements shown in (B).

Author Contributions

Andrea Serfőző: Investigation, Visualization

Gábor András Csík: Investigation, Methodology

Attila Kormányos: Investigation, Visualization, Data curation

Ádám Balog: Investigation, Methodology

Csaba Janáky: Resources, Writing – review & editing, Supervision, Funding acquisition.

Balázs Endrődi: Conceptualization, Data curation, Writing – original draft, Supervision, Funding acquisition.

Conflicts of interest

There are no conflicts to declare.

Acknowledgements

This project has received funding under the European Union's Horizon 2020 research and innovation program from the FlowPhotoChem project (Grant Agreement No. 862453). The research was supported by the National Research, Development and Innovation Office (NKFIH) through the FK-132564 project. B.E. and A.K. also acknowledge financial support by the János Bolyai Research Scholarship of the Hungarian Academy of Sciences and the ÚNKP-22-5 New National Excellence Program of the Ministry for Innovation and Technology from the source of the National Research, Development and Innovation Fund. Project no. RRF-2.3.1-21-2022-00009, titled National Laboratory for Renewable Energy has been implemented with the support provided by the Recovery and Resilience Facility of the European Union within the framework of Programme Széchenyi Plan Plus."

References

- J. Yu, J. Wang, Y. Ma, J. Zhou, Y. Wang, P. Lu, J. Yin, R. Ye, Z. Zhu and Z. Fan, *Adv Funct Mater*, 2021, **31**, 2102151.
- A. Liu, M. Gao, X. Ren, F. Meng, Y. Yang, L. Gao, Q. Yang and T. Ma, *J Mater Chem A Mater*, 2020, **8**, 3541–3562.
- H. Shin, K. U. Hansen and F. Jiao, *Nat Sustain*, 2021, 1–10.
- S. W. Sheehan and R. Buonsanti, *Chem Catalysis*, 2021, **1**, 751–753.
- A. Somoza-Tornos, O. J. Guerra, A. M. Crow, W. A. Smith and B. M. Hodge, *iScience*, 2021, **24**, 102813.
- I. E. L. Stephens, K. Chan, A. Bagger, S. W. Boettcher, J. Bonin, E. Boutin, A. Buckley, R. Buonsanti, E. Cave, X. Chang, S. W. Chee, A. H. M. da Silva, P. de Luna, O. Einsle, B. Endrődi, M. E. Escobedo, J. v. Ferreira de Araujo, M. C. Figueiredo, C. Hahn, K. U. Hansen, S. Haussener, S. Hunegnaw, Z. Huo, Y. J. Hwang, C. Janáky, B. S. Jayathilake, F. Jiao, Z. P. Jovanov, P. Karimi, M. T. M. Koper, K. Kuhl, W. H. Lee, Z. Liang, X. Liu, S. Ma, M. Ma, H.-S. Oh, M. Robert, B. R. Cuenya, J. Rossmeisl, C. Roy, M. P. Ryan, E. H. Sargent, P. Sebastián-Pascual, B. Seger, L. Steier, P. Strasser, A. S. Varela, R. E. Vos, X. Wang, B. Xu, H. Yadegari and Y. Zhou, *Journal of Physics: Energy*, **4**, 042003.
- B. Endrődi, G. Bencsik, F. Darvas, R. Jones, K. Rajeshwar and C. Janáky, *Prog Energy Combust Sci*, 2017, **62**, 133–154.
- D. Wakerley, S. Lamaison, J. Wicks, A. Clemens, J. Feaster, D. Corral, S. A. Jaffer, A. Sarkar, M. Fontecave, E. B. Duoss, S. Baker, E. H. Sargent, T. F. Jaramillo and C. Hahn, *Nat Energy*, 2022, **7**, 130–143.
- T. Burdyny and W. A. Smith, *Energy Environ Sci*, 2019, **12**, 1442–1453.
- Á. Vass, A. Kormányos, Z. Kószó, B. Endrődi and C. Janáky, *ACS Catal*, 2022, **12**, 1037–1051.
- H. Rabiee, L. Ge, X. Zhang, S. Hu, M. Li and Z. Yuan, *Energy Environ Sci*, 2021, **14**, 1959–2008.
- B. De Mot, M. Ramdin, J. Hereijgers, T. J. H. Vlucht and T. Breugelmans, *ChemElectroChem*, 2020, **7**, 3839–3843.
- K. Yang, R. Kas, W. A. Smith and T. Burdyny, *ACS Energy Lett*, 2021, **6**, 33–40.
- H. R. Q. Zhong, F. R. Brushett and P. J. A. Kenis, *Adv Energy Mater*, 2013, **3**, 589–599.
- R. L. Machunda, H. Ju and J. Lee, *Current Applied Physics*, 2011, **11**, 986–988.
- H. Rabiee, X. Zhang, L. Ge, S. Hu, M. Li, S. Smart, Z. Zhu and Z. Yuan, *ACS Appl Mater Interfaces*, 2020, **12**, 21670–21681.
- H. Rabiee, L. Ge, X. Zhang, S. Hu, M. Li, S. Smart, Z. Zhu and Z. Yuan, *Appl Catal B*, 2021, **286**, 119945.
- R. L. Machunda, J. Lee and J. Lee, *Surface and Interface Analysis*, 2010, **42**, 564–567.
- S. Oh, H. Park, H. Kim, Y. S. Park, M. G. Ha, J. H. Jang and S.-K. Kim, *Coatings*, 2020, **10**, 341.
- G. Zhang, Z.-J. Zhao, D. Cheng, H. Li, J. Yu, Q. Wang, H. Gao, J. Guo, H. Wang, G. A. Ozin, T. Wang and J. Gong, *Nat Commun*, 2021, **12**, 5745.
- A. Conte, M. Baron, S. Bonacchi, S. Antonello and A. Aliprandi, *Nanoscale*, 2023, **15**, 3693–3703.
- S. T. Ahn, S. Sen and G. T. R. Palmore, *Nanoscale*, 2022, **14**, 13132–13140.
- P. De Luna, R. Quintero-Bermudez, C.-T. Dinh, M. B. Ross, O. S. Bushuyev, P. Todorović, T. Regier, S. O. Kelley, P. Yang and E. H. Sargent, *Nat Catal*, 2018, **1**, 103–110.



- 24 S. Nitopi, E. Bertheussen, S. B. Scott, X. Liu, A. K. Engstfeld, S. Horch, B. Seger, I. E. L. Stephens, K. Chan, C. Hahn, J. K. Nørskov, T. F. Jaramillo and I. Chorkendorff, *Chem Rev*, 2019, **119**, 7610–7672.
- 25 W. Tang, A. A. Peterson, A. S. Varela, Z. P. Jovanov, L. Bech, W. J. Durand, S. Dahl, J. K. Nørskov and I. Chorkendorff, *Phys. Chem. Chem. Phys.*, 2012, **14**, 76–81.
- 26 F. S. Roberts, K. P. Kuhl and A. Nilsson, *Angewandte Chemie*, 2015, **127**, 5268–5271.
- 27 G. O. Larrazábal, V. Okatenko, I. Chorkendorff, R. Buonsanti and B. Seger, *ACS Appl Mater Interfaces*, 2022, **14**, 7779–7787.
- 28 W. Ye, X. Guo and T. Ma, *Chemical Engineering Journal*, 2021, **414**, 128825.
- 29 T. Möller, F. Scholten, T. N. Thanh, I. Sinev, J. Timoshenko, X. Wang, Z. Jovanov, M. Gliech, B. Roldan Cuenya, A. S. Varela and P. Strasser, *Angewandte Chemie*, 2020, **132**, 18130–18139.
- 30 P. Grosse, D. Gao, F. Scholten, I. Sinev, H. Mistry and B. Roldan Cuenya, *Angewandte Chemie International Edition*, 2018, **57**, 6192–6197.
- 31 P. Grosse, A. Yoon, C. Rettenmaier, A. Herzog, S. W. Chee and B. Roldan Cuenya, *Nat Commun*, 2021, **12**, 6736.
- 32 S. Popović, M. Smiljanić, P. Jovanović, J. Vavra, R. Buonsanti and N. Hodnik, *Angewandte Chemie*, 2020, **132**, 14844–14854.
- 33 D. T. Whipple, E. C. Finke and P. J. a. Kenis, *Electrochemical and Solid-State Letters*, 2010, **13**, B109.
- 34 B. Kim, S. Ma, H.-R. Molly Jhong and P. J. A. Kenis, *Electrochim Acta*, 2015, **166**, 271–276.
- 35 N. Kumar, G. D. Varma, R. Nath and A. K. Srivastava, *Applied Physics A*, 2011, **104**, 1169–1174.
- 36 G. F. Samu, C. Visy, K. Rajeshwar, S. Sarker, V. R. Subramanian and C. Janáky, *Electrochim Acta*, 2015, **151**, 467–476.
- 37 B. Endrődi, A. Samu, E. Kecsenovity, T. Halmágyi, D. Sebők and C. Janáky, *Nat Energy*, 2021, **6**, 439–448.
- 38 B. Endrődi, G. F. Samu, D. Fejes, Z. Németh, E. Horváth, A. Pisoni, P. K. Matus, K. Hernádi, C. Visy, L. Forró and C. Janáky, *J Polym Sci B Polym Phys*, 2015, **53**, 1507–1518.
- 39 A. A. Samu, A. Kormányos, E. Kecsenovity, N. Szilágyi, B. Endrődi and C. Janáky, *ACS Energy Lett*, 2022, **7**, 1859–1861.
- 40 A. Kormányos, B. Endrődi, Z. Zhang, A. Samu, L. Mérá, G. F. Samu, L. Janovák and C. Janáky, *EES Catalysis*, 2023, **1**, 263–273.
- 41 R. M. Arán-Ais, R. Rizo, P. Grosse, G. Algara-Siller, K. Dembélé, M. Plodinec, T. Lunkenbein, S. W. Chee and B. R. Cuenya, *Nat Commun*, 2020, **11**, 1–8.

